PERGAMON

International Journal of Heat and Mass Transfer 44 (2001) 2567–2581

International Journal of HEAT and MASS TRANSFER

www.elsevier.com/locate/ijhmt

Soot processes in a methane-fueled furnace and their impact on radiation heat transfer to furnace walls

Salah-Addin B. Al-Omari [a,b,*], Kazuhiko Kawajiri [a], Takashi Yonesawa [a]

[a] *Combustion & Surface Chemistry Group, Energy Technology Department, Mitsubishi Electric Corporation, Advanced Technology R & D Center, 8-1-1 Tsukaguchi-Honmachi, Amagasaki City, Hyogo 661-8661, Japan*

[b] *Mechanical Engineering Department, United Arab Emirates University, College of Engineering, AL-AIN, United Arab Emirates*

Received 23 July 1999; received in revised form 31 March 2000

Abstract

Soot process in a vertical methane-fueled furnace supplied with fuel through its primary inlet located at its bottom, and with air via two opposing horizontal air jets perpendicular to the direction of fuel supply, are studied numerically under different operating conditions. Results show that increasing the inlet temperature of fuel and/or air favors soot generation, hence enhances thermal radiation to walls. Radiation to the walls also increases by increasing air supply rates under fixed overall excess air ratio (EAR) conditions. Increasing EAR favors soot formation in the circulating regions formed below air jets, but it enhances soot oxidation in the upper locations. Consequently the heat radiated to walls is reduced.

1. Introduction

Soot represents an important pollutant. Its emission from any combustion device means a reduction in the thermal efficiency of that device. However, the presence of soot in a combustion chamber enhances heat transfer by radiation to chamber walls, which is a desirable effect for example in boilers. Therefore, the production of soot in proper places inside the combustion chamber, and making sure to oxidize it before exiting to the atmosphere represents an important aspect in the design of boilers. In addition to the importance of controlling soot formation from the point of view of heat transfer to furnace walls, the control of soot formation is also very important in relation to the radiation cooling of the active NO_x producing hot sites, which is enhanced significantly by the presence of soot particles.

The present paper focuses on the numerical study of the effect of different furnace operation parameters on soot processes and radiation heat transfer to furnace walls. Hereby a vertical methane-fueled furnace supplied with fuel through its primary inlet located at its bottom, and with air via two horizontal air jets issuing from two opposing rectangular slots (see Fig. 1), is considered.

The flow field and combustion characteristics under the boundary conditions considered in this study result in interesting and unique features of soot formation processes. The fuel considered is methane. Although under atmospheric pressure diffusion flame conditions methane is known to be a weak sooting fuel, a fact which might justify the commonly adopted approach of decoupling the gas phase computations from soot, simulation results showed that relatively high amounts of soot are generated from methane. This, as will be seen in the results section, is attributed to the flow field and combustion characteristics of the furnace under consideration.

Under such soot generation favoring conditions, particularly when more sooty fuels other than methane are used, soot can no longer be treated as a small perturbation on the gas phase. Hence, decoupling the gas phase computations from soot can clearly lead to inaccurate simulation results. The main feature of decoupling which is of main interest to us here is neglecting the depletion of fuel due to fuel/soot conversion. This

* Corresponding author. Tel.: +971-3-7051307; fax: +971-3-7623158.

E-mail address: s.omari@uaen.ac.ae (S.-A.B. Al-Omari).

0017-9310/01/$ - see front matter
PII: S0017-9310(00)00288-X

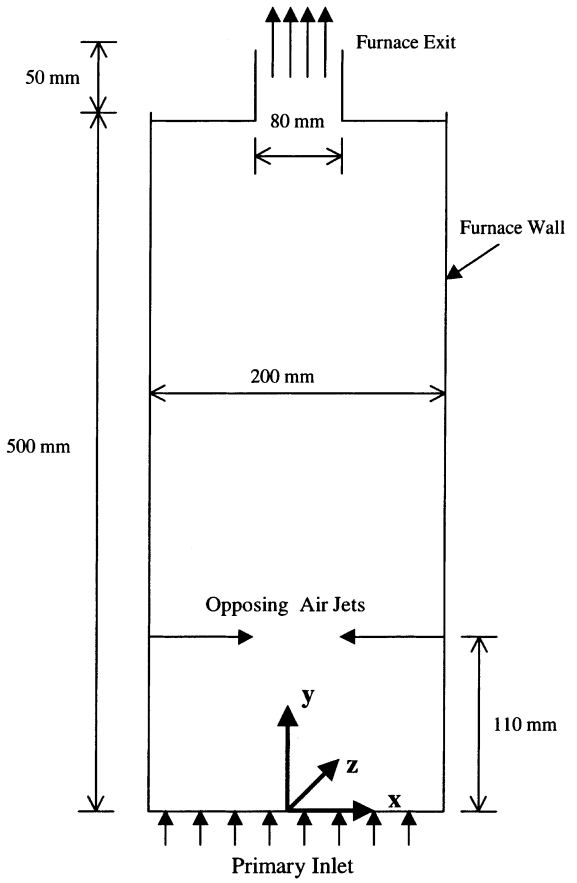

Fig. 1. Two-dimensional schematic diagram of the simulated furnace.

might be reflected directly on the prediction of the spatial distribution of species concentrations (including soot) and temperatures, hence on thermal radiation transport in the furnace.

The characteristics of soot formation activity in the present furnace, particularly in the vortices formed between the air jets and the primary inlet, are found to be very dependent on the adopted operating conditions. Therefore the study investigates soot formation and the heat radiated to the walls under different operating conditions. Depending on the significance of soot formation activity under these operating conditions, inferred from the present computations, one might get an insight into the possible drawbacks in the numerical predictions that can result when the assumption of decoupling the gas phase from soot is adopted in the simulation. Further investigation of this point with regard to radiation heat transfer and to NO_x formation under boundary conditions similar to those considered in this paper will be addressed in a subsequent research work. In the present study coupling between the gas phase and soot is accounted for in the way described in the next section.

The furnace operation parameters considered in this paper are: (1) increasing the inlet temperature of both combustion air and fuel, (2) increasing the overall EAR, and (3) increasing the total mass flow rate of both air and fuel supplied to the furnace, under constant EAR conditions (i.e., increasing the output thermal power under fixed EAR conditions).

2. Mathematical and physical formulation

This investigation is based basically on our recent research work [1], with, however, a modification to the representation of the path of soot generation. The employed modeling strategy is described below.

The soot inception, surface growth and coagulation processes are stimulated using soot model developed by Syed et al. [2]. This model stimulates the processes mentioned above by means of source/sink terms added to the conservation equations of two soot representative quantities, namely the soot number density (particles/unit volume) and soot volume fraction. Oxidation of soot is stimulated by the model of Nagle–Strickland–Constable (NSC) [3]. Here soot is assumed to be oxidized by oxygen molecules.

The NSC model has been shown to correlate graphite and soot oxidation over a wide range of temperatures and concentrations [4,5]. Moreover, a comparison between experimental and computational results of the steady CH_4–air flame shows that the NSC rate expression performs in a satisfactory way, particularly regarding the prediction of the soot burnout height and the overall flame shape [6]. These points, in addition to noting that results of the present work and conclusions drawn from them are not expected to be affected significantly by the oxidation model adopted, encouraged us in this study to employ the NSC model to simulate soot oxidation. The surface oxidation rate (g cm^{-2} s^{-1}) of a soot particle according to the NSC model is given as

$$W_{\mathrm{NSC}} = 12\left[\frac{k_{\mathrm{A}}P_{\mathrm{O}_2}}{1+k_z P_{\mathrm{O}_2}}\chi + k_{\mathrm{B}}P_{\mathrm{O}_2}(1-\chi)\right] \tag{1}$$

where P_{O_2} is the partial pressure of oxygen (atm),

$$\chi = \frac{1}{1+(k_T/K_{\mathrm{B}}P_{\mathrm{O}_2})}.$$

For empirical rate parameters in the NSC-model appearing in Eq. 1, see for example [3]. It should be noted that multiplying the oxidation rate expression as given in the original paper of Nagle and Strickland–Constable [3] by 12 (the molecular weight of carbon) gives the oxidation rate in the unit of g/cm^2 s (see Eq. (1)).

The methane flame soot model of Syed et al. is a simple representation of the soot formation process, which reproduces to a satisfactory extent soot concentrations obtained experimentally. Most importantly, however, it accounts to a satisfactory extent for the variation of soot concentrations with residence time at a fixed mixture fraction. The model has been adopted to model soot formation in flickering flames [6]. Thereby, the model successfully predicted the overall enhancement of the soot volume fraction observed experimentally. This success led Kaplan et al. [6] to identify, as compared with steady flames, the extended residence time of soot particles in soot favoring regions in flickering flames as the most important parameter affecting increased soot production. In the present study, configuration of the flowfield is different from that of the laminar flame in the experiments of Syed et al. [2]. Of main significance here is the extended residence time of soot particles (the effect of which on surface growth, seemingly, is accounted for properly by the model), in the fuel-rich hot regions in the lower part of the furnace close to the primary inlet (cf. Section 3).

The combustion rate of methane is simulated by the eddy dissipation concept of Magnussen et al. [7]. Radiation heat transfer in the furnace is simulated by the 'discrete transfer method' [8]. The gas is assumed to be of the 'gray body' type. The effect of the soot, which is usually the dominant radiating species in the hydrocarbon-fueled flames [9], on radiation transfer is accounted for by using a combination of the empirical formula of Kent and Honnery for soot [10], and that of Magnussen and Hjertager for CO_2 and H_2O [7] to determine the overall Planck mean absorption coefficient, which is then given as [6]

$$\text{Absorbtion coefficient} = 2.66 \bullet \text{const} \bullet f_v \bullet T + 0.001(X_{CO_2} + X_{H_2O})\ \text{cm}^{-1}, \tag{2}$$

where X_{CO_2} and X_{H_2O} are the mole fractions of CO_2 and H_2O, respectively. The constant used in this equation is equal to 7.0 [10].

The walls in the radiation computations are taken to be of the gray Lambert type and the reflection to be diffuse. The emissivity and reflectivity coefficients of the wall are taken to be 0.4 and 0.6, respectively.

In order to account for the contribution of soot combustion to the overall heat releasing reactions, soot is assumed to be in the form of solid carbon, oxidation of which leads eventually to the formation of carbon dioxide. The existence of hydrogen atoms in soot particles is neglected. However, negligence of hydrogen in the intermediate hydrocarbons taking part in soot formation processes might under conditions of intensive soot generation lead to a nonnegligible under-prediction of the total heat released from a certain quantity of fuel entering the furnace, as well as to an artificial increase in the amounts of oxygen available for combustion. Moreover, this would lead to an under prediction of the concentration of water vapor generated by the oxidation processes, which is an important gaseous species from the point of view of thermal radiation transport. Therefore, although it is a rough approximation, the path of fuel/soot conversion adopted here is assumed to be as follows:

Fuel → soot in the form of solid carbon + hydrogen molecules

The oxidation of hydrogen is represented by the mixing model of Manussen et al. [7]. The influence of soot generation and soot oxidation on, respectively, the fuel and oxygen concentration is accounted for by a sink term added to the conservation equation of each of these species. A source term due to soot oxidation is added to the CO_2 conservation equation. Another source term due to hydrogen oxidation is added to the conservation equation of H_2O.

In order to account for the effect of turbulent temperature fluctuations on soot generation a simple probability density function (PDF) for temperature composed of two delta functions located at $\overline{T} \pm (\overline{T'^2})^{1/2}$, is employed. The effects of the fluctuations of the parent fuel concentration on soot processes are ignored, the mean value of fuel concentration is used in the present soot calculations.

Local values of the temperature variance ($g_T = \overline{T'^2}$) are obtained by solving a transport equation for this quantity. This equation has the following general modeled form:

$$\frac{\partial}{\partial t}(\rho g_T) + \frac{\partial}{\partial x_j}\left[\rho \overline{u}_j\, g_T - (\Gamma_{g,\text{eff}})\frac{\partial g_T}{\partial x_j}\right] = 2\frac{\mu_t}{\sigma_{g_T}}\left(\frac{\partial \bar{T}}{\partial x_j}\right)^2 - C\rho\frac{\varepsilon}{k}g_T + \bar{S}, \tag{3}$$

where σ_{g_T} and C have values 0.7 and 2.0, respectively. In this equation S represents a source/sink term due to interaction between the turbulent temperature fluctuations and both the heat releasing reactions as well as the heat loss caused by radiation cooling and endothermic soot formation reactions. In this study, however, $\bar{S}$ is not considered in the simulations. It should be noted that, temperature variance equation in the form given by Eq. (3) is based on a transport equation written for temperature under the assumption of a unity Lewis number, equal specific heats for all species, and negligible spatial gradients of the specific heat.

In the numerical program employed in the computations, mass, momentum, species and energy equations, in addition to two transport equations for the soot number density and soot volume fraction, as well as an

Table 1
Main boundary conditions

Case No.	EAR	Air velocity (m/s)	Air temp. (K)	Primary gas velocity (m/s)	Primary gas temp. (K)
1 [a]	1.15	8.22	350	0.15	600
2	1.15	9.35	400	0.15	600
3	1.15	8.22	350	0.090	350
4	1.6	11.73	350	0.15	600
5	1.15	16.45	350	0.30	600

[a] Base case.

equation for the temperature variance, are solved by a finite volume method using an upwind scheme. The numerical solution follows the SIMPLE algorithm. Turbulence closure is affected by the standard k–ε model. A mixture of ideal gases is assumed. The variation in the thermophysical properties with temperature and concentration is accounted for. Molecular diffusivity of soot particles is neglected in the diffusion terms in the transport equations of soot number density and soot volume fraction as compared with the effects of turbulent transport.

The furnace considered here (see Fig. 1) is supplied with air via two air jets issuing from two opposing rectangular slots (with width of 5 mm) extending along the furnace wall in the direction of the furnace depth; the z-direction in Fig. 1. The furnace has a width of 20 cm and a height of 55 cm. This type of secondary air injection ports, as a result of the symmetry of any cross-section parallel to the x–y plane in Fig. 1, allows for performing simple two-dimensional calculations which yet still give significant insights into the combustion and soot processes taking place under flow boundary conditions in which opposing air jets make a cross flow with the main direction of the gas flow in the furnace. Moreover, the geometrical symmetry of the adopted 2D cross-section about its central vertical axis allows for adopting only one half of the cross-section to perform the calculations.

3. Results and discussion

Fig. 1 shows a 2D schematic diagram of the simulated furnace. The distribution inside the furnace of the different properties of interest to us in this study will be presented in the form of contours in one half of the 2D-cross-section presented in Fig. 1. The main boundary conditions adopted in each of the cases studied are summarized in Table 1. In all cases mass composition of the primary gas entering the furnace through its primary inlet, which can be thought of as a porous plate issuing a uniform velocity gas, is taken to be 30% CH_4 and 70% N_2. Wall temperature is fixed at 800 K. In all cases inlet turbulence intensity of the combustion air is taken to be 3%. The furnace is operated under atmospheric pressure. In Table 1 in order to distinguish the different cases from case 1 (the base case), the distinguishing boundary condition is put a small box.

In the first stage of the discussion the results of case 1 are presented. After this the influence of increasing the temperature of combustion air on combustion and soot processes is studied (case 2). Subsequently the discussion covers the effect of decreasing the temperature of the primary gas (case 3). In a later stage the effect of increasing the amount of combustion air introduced to the furnace (i.e. increasing the overall EAR) is investigated (case 4). Finally, in case 5 the mass flow rates of both primary gas and combustion air are doubled; EAR is kept constant at 1.15 as in case 1.

4. Base case (case 1)

Case 1 represents the base case with which all other subsequent cases are compared. Therefore, the results of this case are discussed here in detail. Fig. 2(a) shows the velocity vectors corresponding to case 1; half cross-section is shown in the figure. The horizontal combustion air jets issuing from the two opposing air slots entrain some of the gas in their vicinity as they penetrate towards the central region of the furnace. Eventually they hit each other at a midway location between them. Thereby, a stagnation point-like flow region is formed. Some of the gas entering this stagnation point region flows subsequently downward towards the primary inlet, while the other part flows upward along the y–z symmetry plane. The downwardly flowing part attacks the gases issuing upward forming a second stagnation point flow region close to the primary inlet. This flow scenario leads to the generation of two pairs of symmetrical circulating motions inside the furnace. One upper pair having its two symmetrical vortices extending from regions located directly above the air jets, along the furnace side walls. The other lower pair has two symmetrical vortices with their centres being located roughly 2 cm off the central y–z symmetry plane, about 9 cm above the primary inlet of the furnace. The coordinates of the centres of circulating motions are however

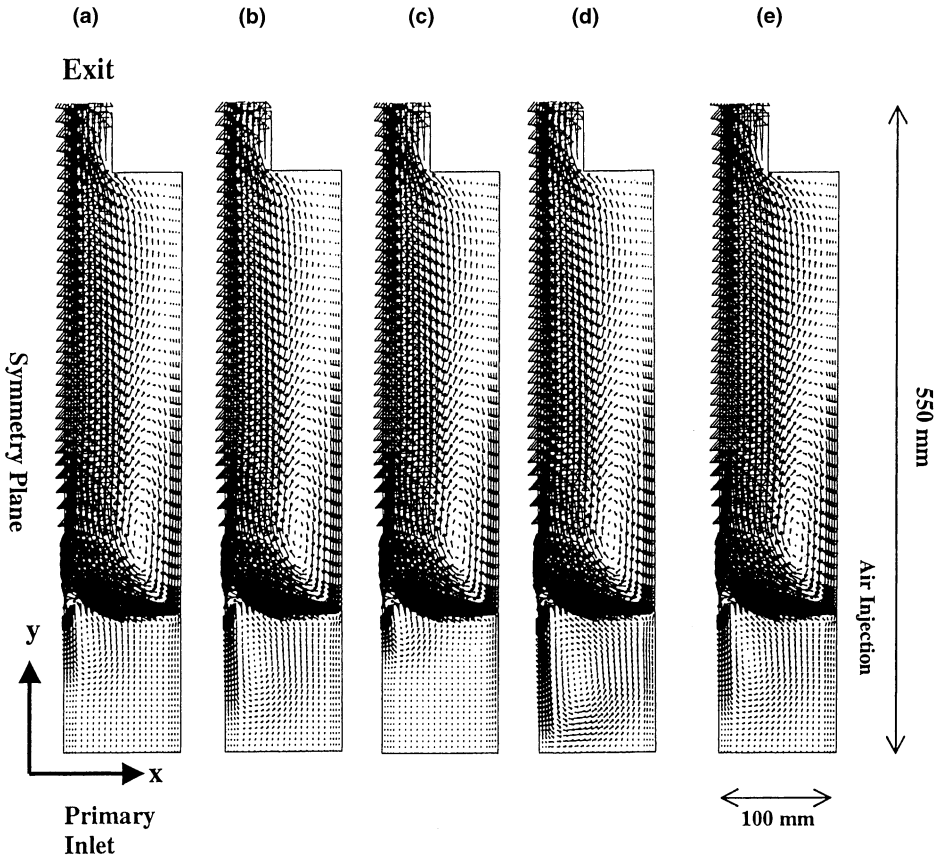

Fig. 2. Velocity vectors plot: (a) case 1; (b) case 2; (c) case 3; (d) case 4; (e) case 5.

dependent on the operating boundary conditions of the furnace (cf. Fig. 2).

Practically no oxygen can survive and reach the stagnation point flow region between the two air jets before having been either consumed by the fuel or deflected upward to flow in the upper regions of the furnace (cf. equivalence ratio contours; Fig. 3(c)). Hence, gas issuing from the stagnation point region in the downward direction towards the primary inlet will be mostly a mixture of combustion products, nitrogen, and unburned combustible components (fuel and soot). This relatively hot mixture contributes to heating the regions below the stagnation point. Heat is transmitted subsequently, via the circulatory motion, conduction and thermal radiation to other parts in the primary inlet (PI)-region. Some of the fuel (including soot) circulating in the PI-region, which is entrained into the air jets, will be circulated towards the stagnation point flow region, and from there flows upward along the y–z symmetry plane while it burns under turbulent diffusion flame conditions (cf. Figs. 3(a) and (c)). Of course some part of the soot flowing in the upper part of the furnace is generated originally in upper locations along the y–z plane, where temperatures and fuel concentrations are high enough to support soot formation activities (cf. Figs. 3(d) and (e)).

The reduction in methane concentration in the region below the stagnation point, observed in Fig. 3(b), is mainly a consequence of the dilution caused by the hot gaseous mixture issuing from the stagnation point region in the downward direction. The contribution of fuel/soot conversion processes to this reduction in methane concentration is of lower significance. This can be confirmed from the comparatively low amounts of soot in Fig. 3(e). The depth in the y-direction below the stagnation point, over which fuel concentration dilution is clearly observable, can be considered as an indicator of the penetration strength of hot gases expelled from the stagnation point region in the downward direction.

Maximum soot number density in Fig. 3(d) is found along the y–z plane about 30 cm above the primary inlet and 7 mm off the y–z symmetry plane, at temperatures roughly between 1600 and 1700 K, and under equivalence ratio levels >2.0 (cf. Figs. 3(a), (c) and (d)). As soot particles approach fuel-leaner boundaries of the equivalence ratio contours oxidative attack on their surfaces becomes important leading to decreasing their size, and

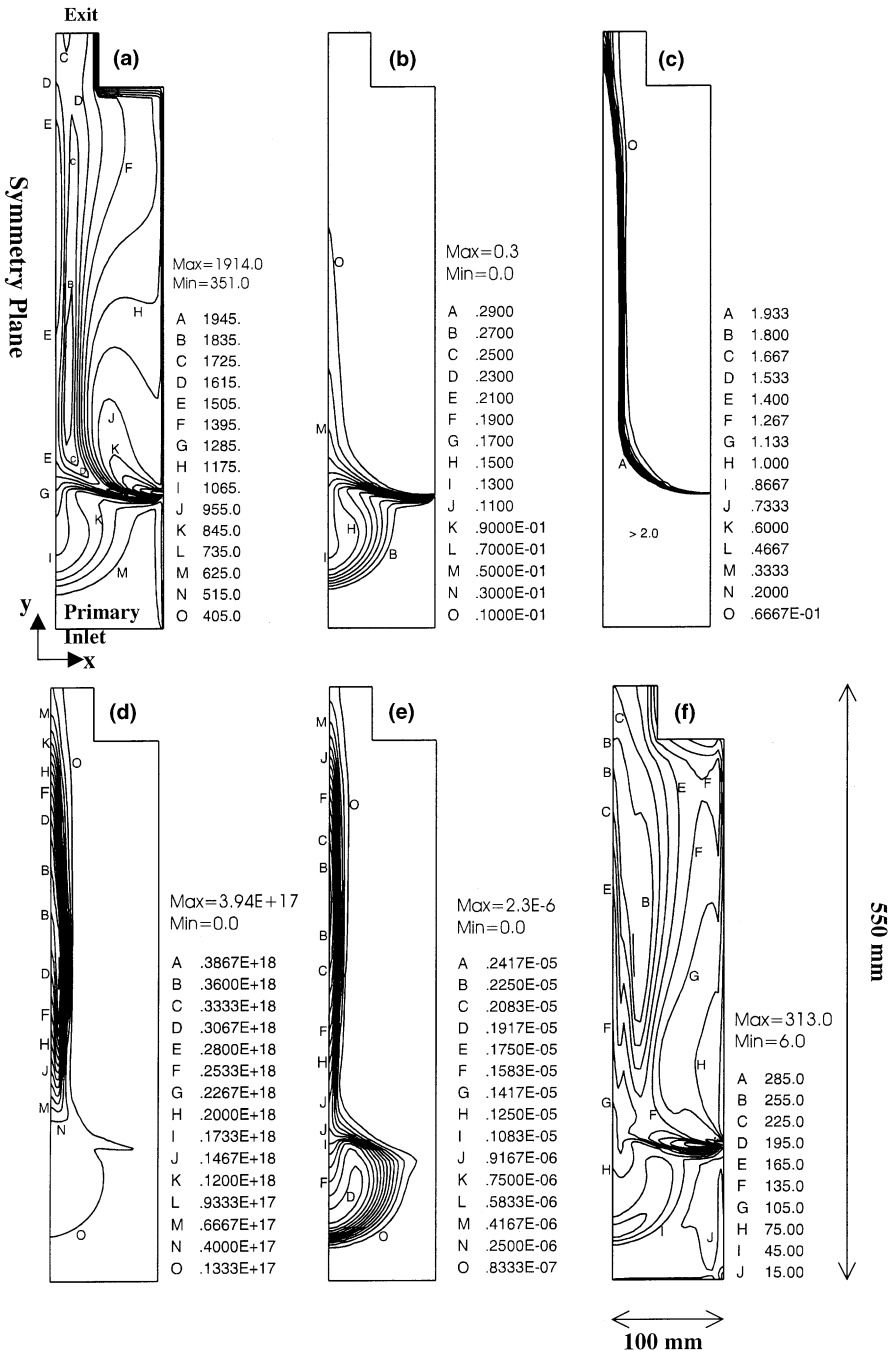

Fig. 3. Results for case 1: (a) temperature (K); (b) CH_4 mass fraction; (c) CH_4 equivalence ratio; (d) soot number density (part./ m^3); (e) soot volume fraction; (f) $(\overline{T'^2})^{1/2}$.

consequently to a reduction in the soot number density and soot loading in these locations (cf. Fig. 3(d) and (e)).

The sites of highest soot volumes fractions (around 2.3×10^{-6}) are found to be located almost directly at the y–z symmetry plane, about 36 cm above the primary inlet (cf. Fig. 3(e)). High soot volume fractions (as high as 2.0×10^{-6}) are also found within the circulating regions in the PI-region. It should be noted that peak soot volume fraction levels attained under the flow and combustion conditions of the present furnace are noticeably higher than those typical for normal methane diffusion flames operating under atmospheric pressure.

Along the y–z plane the high soot loading is attributed to two main factors: first to the intensive inception and surface growth reactions taking place on the surfaces of the generated soot particles; secondly, to the amounts of soot circulated from the PI-region upward. On the other hand, in the vortices of the PI-region (in which, as a result of their comparatively low temperatures, no soot inception takes place), the relatively high soot loading is attributed to soot particles circulated from the stagnation point region downward, which as a result of the circulatory motion subsequently reside for a relatively long time in the PI-region, under hot fuel-rich soot generation favoring conditions.

The favoring role played by turbulent temperature fluctuations concerning soot generation can be appreciated by considering Fig. 3(f), which shows the distribution of the rms of the temperature variance, $(\overline{T'^2})^{1/2}$. In the stagnation point region between the two air jets, as well as in the hottest fuel-rich sites of the PI-region, $(\overline{T'^2})^{1/2}$ attains values roughly between 75 and 135 K. According to the soot model of Syed et al., for two representative values of the mean temperature under fixed fuel concentration conditions, for example 1400 and 1800 K which are similar to temperatures characterizing the stagnation point region and the hottest sites along the y–z plane, the soot inception rate increases by about 800% and 300%, respectively, when the temperature increases due to turbulent fluctuations by 100 K above the mean value. An equivalent reduction in temperature below the mean (i.e., -100 K) would however lead to a corresponding reduction in soot inception rate of only about 90% and 80%, respectively. The rate of surface growth is also enhanced by turbulent temperature fluctuations. Under fixed fuel concentration conditions, and for two representative values of the mean temperature, for example 1400 and 1000 K which are similar to temperatures characterizing the stagnation point region and closely below it, the soot model predicts an increase in surface growth rate of about 90% and 230%, respectively, when the temperature increases as a result of turbulent fluctuations by 100 K. A reduction in temperature of 100 K below the mean value would however lead to a corresponding reduction in the soot production rate via surface growth reactions of about 52% and 77%, respectively. The above numerical examples highlight a clear favoring role played by turbulent temperature fluctuations concerning soot formation.

5. Effect of increasing secondary air temperature (case 2)

In this section case 2 is studied. Hereby, as compared with case 1, the injection temperature of combustion air is increased by 50 K (see Table 1). The flowfield characteristics of case 2 (Fig. 2(b)) are qualitatively similar to those of case 1 (Fig. 2(a)). In the upper part of the furnace, above the air jets, both cases are even quantitatively very close to each other. In the PI-region, however, there are some clear quantitative deviations between the two cases, which have clear consequences on soot and gas phase characteristics. In case 2, the higher injection velocity of the combustion air (air injection density in case 2 is slightly lower than that in case 1 because of the increase in injection temperature in the former case) leads to higher amounts of hot combustion products being circulated from the stagnation point flow region in the downward direction. Accordingly, the resulting circulating motions in the PI-region in case 2 are stronger and occupy a larger space. Moreover, from Figs. 3(a) and 4(a) a discerning eye can tell of higher temperatures in case 2 in the contact sites between fuel and air jets, and in the stagnation point region, which are due to higher injection-temperature of air in this case, as well as higher injection velocity which enhances mixing and hence combustion rates. This leads to higher soot inception rates in the fuel-rich side of the air jets and in the stagnation point region (cf. Figs. 3(d) and 4(d)). Consequently, in case 2 a higher number of soot precursors are circulated from the stagnation point region downward into the PI-region. This, in addition to enhancement in local temperatures in the PI-region caused by higher amounts of hot gases circulated downward, leads to a clear increase in the amount of soot generated in the PI-region in case 2 (cf. Figs. 3(e) and 4(e)). It should be noted that this enhancement in soot production rates in the PI-region is countered by the negative influence of the dilution of the fuel concentration caused by hot gas entering the PI-region from the stagnation point region, which is more pronounced in case 2 (cf. Figs. 3(b) and 4 (b)). Apparently, however, the higher soot number densities, higher temperatures, and higher level of turbulent temperature fluctuations in case 2 (particularly in the hottest sites of the PI-region, cf. Figs. 3(f) and 4(f)), have a favoring effect on soot formation which far exceeds the depressing role played by fuel concentration dilution.

In contrast to case 1, locations of highest soot number density along the y–z plane do not coexist with those corresponding to highest soot volume fractions; highest soot volume fractions (around 2.9×10^{-6}) in case 2 are found in the vortices of the PI-region which are characterized by comparatively low soot number densities (cf. Figs. 4(d) and (e)). In case 2 soot particles spend a long enough time in the circulating regions below the air jets, under soot generation favoring conditions, rendering peak soot volume fraction levels in case 2 (2.9×10^{-6}) even higher than those attained in case 1 (2.3×10^{-6}) along the y–z plane.

Irrespective of the higher total amounts of soot generated in case 2, more soot is emitted from the furnace in case 1. The lower soot emission in case 2 can be

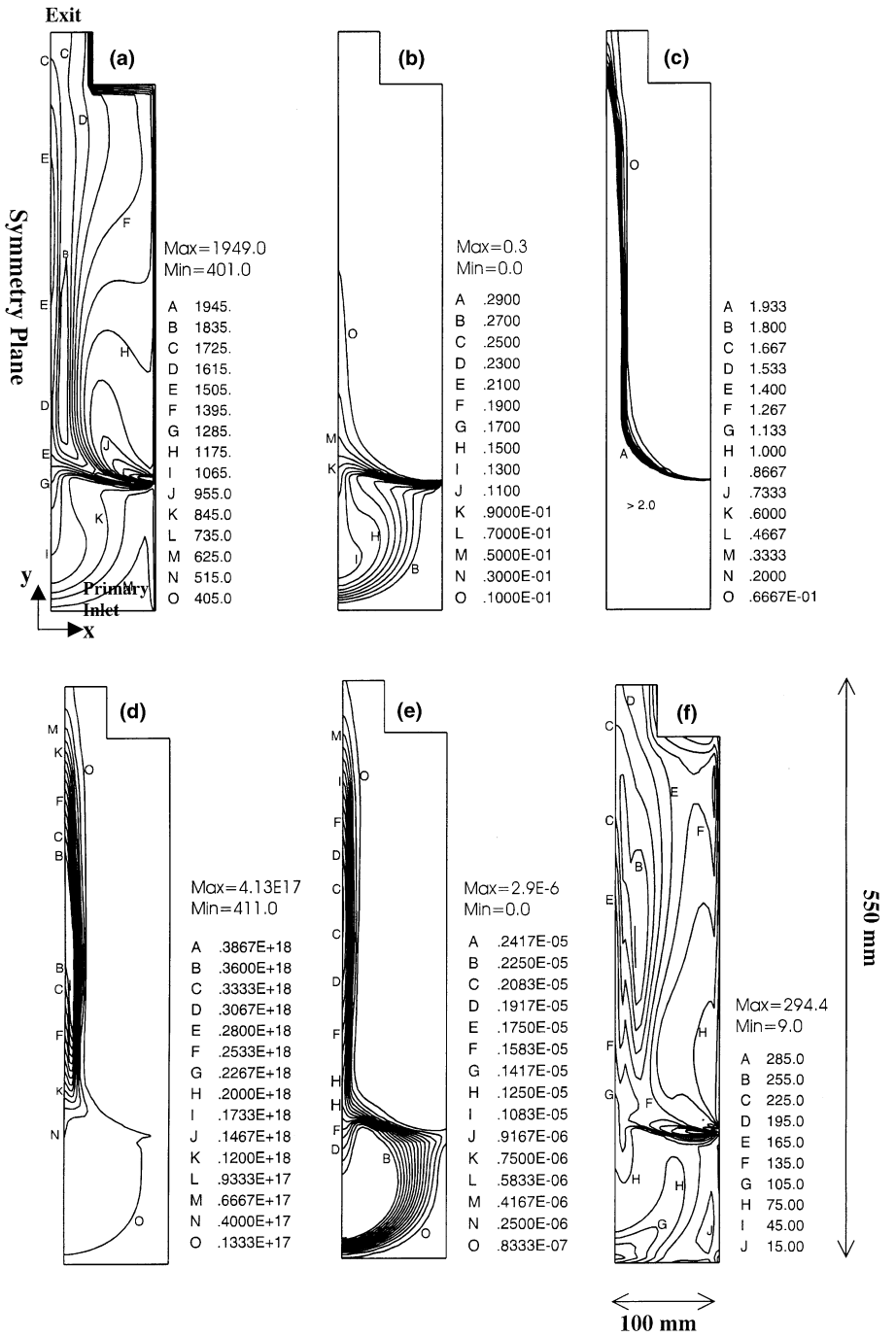

Fig. 4. Results for case 2: (a) temperature (K); (b) CH_4 mass fraction; (c) CH_4 equivalence ratio; (d) soot number density (part./m^3); (e) soot volume fraction; (f) $(\overline{T'^2})^{1/2}$.

explained by noting the higher local temperatures in the hot oxidizing sites along the y–z plane in this case (cf. Figs. 3(a) and 4(a)), which are partly due to the higher air injection temperature. This leads to a more effective soot oxidation. Moreover, in case 2 the higher air injection velocities enhance mixing and fuel combustion rates, which consequently results in higher temperatures, and at the same time lower local concentrations of the fuel; methane represents here the driving species for soot formation. As can be seen in Fig. 3(c) and Fig. 4(c),

more unburned fuel escapes the furnace in case 1. This is in part due to the higher total amounts of fuel converted to soot in the PI-region in case 2.

To facilitate a simplified means for comparison between different cases considered in this study a one-dimensional plot showing the distribution of soot volume fraction along the y–z plane for all cases is presented in Fig. 5. Moreover, to see the consequences of these different soot distribution characteristics on radiation heat transfer, the flux of incident thermal radiation at the furnace wall is presented in Fig. 6 as a function of distance along the wall.

As seen from Fig. 5, in case 2 clearly higher amounts of soot are present up to about 27 cm above the primary inlet. Above this height the amounts of soot in case 1 surpass those corresponding to case 2. A decline in the soot volume fraction in the stagnation point region between the two air jets is quite clear.

From Fig. 6 it can be seen that up to about 40 cm above the primary inlet heat radiated to the walls in case 2 is clearly higher than that in case 1. This is mainly due to the higher temperatures, and to some extent higher

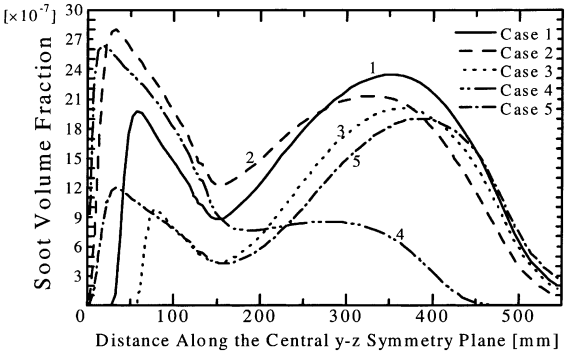

Fig. 5. Soot volume fraction along the central y–z symmetry plane.

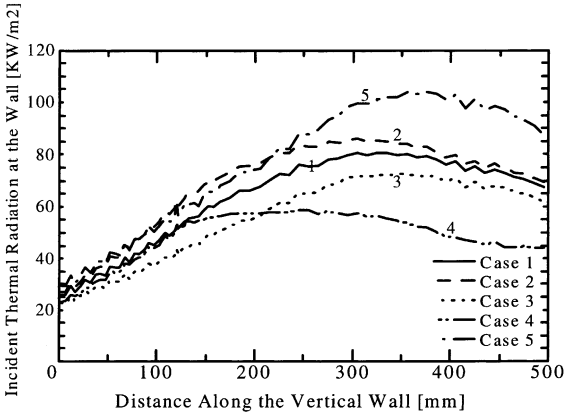

Fig. 6. Incident thermal radiation flux at the furnace wall.

amounts of soot present in the hot sites over about 27 cm above the primary inlet in case 2 (cf. Figs. 3–5). Although soot amounts in case 1 at heights above 27 cm are higher, the lower local temperatures in this case render radiation flux at these heights somewhat lower than that corresponding to case 2.

6. Effect of decreasing the temperature of the primary gas (case 3)

In this subsection the influence of reducing the temperature of the fuel-bearing gas entering the furnace through its primary inlet (case 3; see Table 1) on combustion and soot characteristics in the furnace is highlighted. The results for this case are presented in Figs. 2(c) and 7.

The main difference between cases 3 and 1 lies in the flowfield in the lower part of the furnace (the PI-region). In case 3, as a result of the higher density of the primary gas due to its lower temperature, the hot gases expelled from the stagnation point region penetrate a shorter distance in the downward direction. Hence, the hot circulating regions below the air jets are clearly smaller than those corresponding to case 1 (cf. Figs. 2(a) and 2(c)). Accordingly, the size of the region in which soot is effectively generated is significantly reduced (compare Figs. 3(e) and 7(e)). The reduction in temperature in the contact sites between fuel circulating in the PI-region and the air jets, which is in part a result of the lower primary gas temperature, leads to a reduction in the soot inception rates in these sites, as well as in the stagnation point region (cf. Figs. 3(d) and 7(d)). This represents an important factor leading to a noticeable reduction in the total amounts of soot generated in the PI-region in case 3.

In the upper region above the air jets the flow and combustion characteristics, both qualitatively and to a great extent quantitatively, are the same in both cases 1 and 3. However, since local temperatures in both cases are quite the same, it might be inferred from the clearly lower amounts of soot along the y–z plane in case 3 (cf. Fig. 5), that in this case less heat is radiated to the furnace walls. This, indeed, is confirmed by Fig. 6.

7. Effect of increasing overall EAR (case 4)

In this section case 4 is discussed (EAR = 1.6; see Table 1). The results are presented in Figs. 2(d) and 8. The general features of the flowfield of case 4 are similar to those of the other cases studied so far. However, in case 4, as a result of higher air injection velocity, more hot gas is circulated downward toward the primary inlet of the furnace, forming stronger circulating currents in the PI-region; compare the velocity vectors of case 4

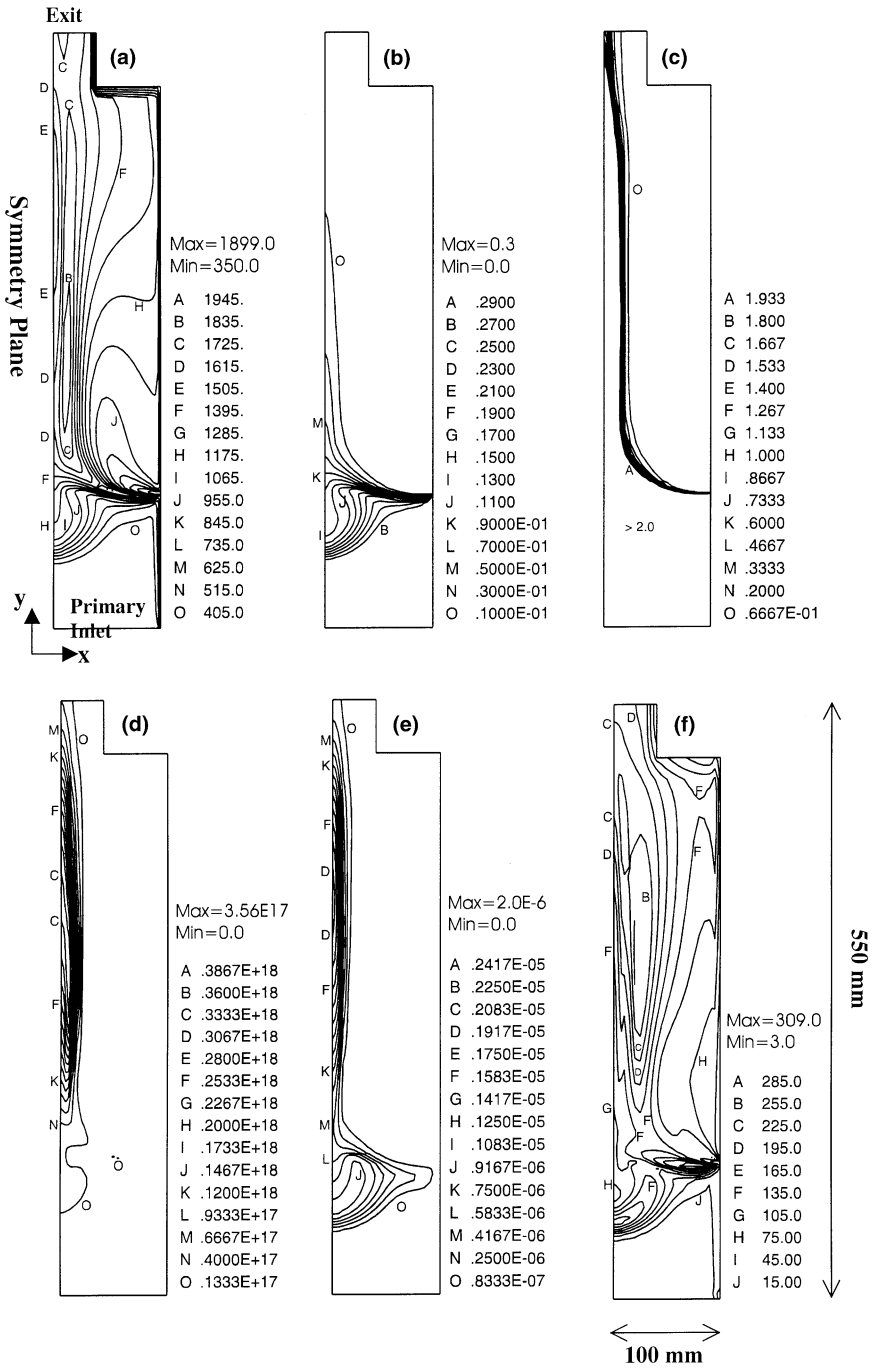

Fig. 7. Results for case 3: (a) temperature (K); (b) CH_4 mass fraction; (c) CH_4 equivalence ratio; (d) soot number density (part./m^3); (e) soot volume fraction; (f) $(\overline{T'^2})^{1/2}$.

(Fig. 2(d)) with those corresponding to case 1 (Fig. 2(a)). In the upper part of the furnace, the flow field is to a high extent similar in all cases studied so far; of course with higher absolute velocities in case 4 due to higher amounts of gas flowing in the furnace in this case.

As compared with case 1, due to the higher air injection velocity in case 4 more intensive turbulent combustion takes place in the contact sites between the fuel and the air, leading to higher temperatures in these sites. Furthermore, in case 4 locations of highest temperatures

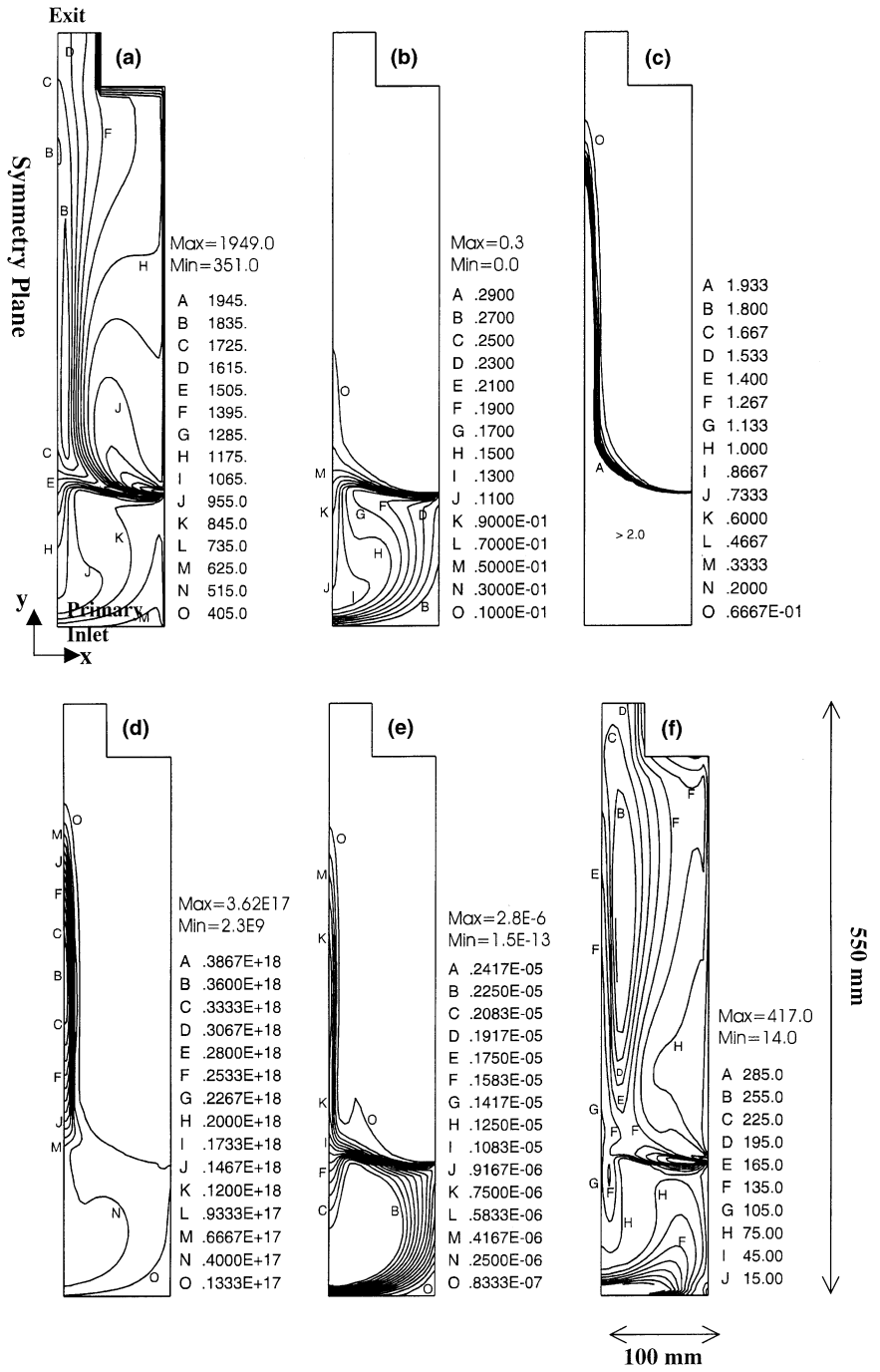

Fig. 8. Results for case 4: (a) temperature (K); (b) CH_4 mass fraction; (c) CH_4 equivalence ratio; (d) soot number density (part./m^3); (e) soot volume fraction; (f) $(\overline{T'^2})^{1/2}$.

along the y–z plane are shifted further downward toward the stagnation point region. At the furnace exit, however, the higher amounts of air introduced to the furnace in case 4 lead to lower temperatures (cf. Figs. 3(a) and 8(a)).

The higher local temperatures in case 4 in the fuel-rich stagnation point region lead to higher soot inception rates. Consequently, the number of soot precursors transferred from the stagnation point region downward,

is clearly increased (cf. Figs. 3(d) and 8(d)). This factor, in addition to the higher local temperatures in the PI-region along the y–z plane, leads to much higher fuel/soot conversion rates in the vortices of the PI-region in case 4 (cf. Figs. 3(e) and 8(e)). It should be noted that higher amounts of hot gases circulated downward in case 4 lead to a more pronounced dilution of fuel concentrations in the hot sites below the stagnation point region (cf. Figs. 3(b) and 8(b)). The adverse effect of this factor on soot generation, however, is seen to be more than countered by the favoring effect of the higher local temperatures and the increased soot number densities in the stagnation point region, and closely below it. Moreover, in this regard the positive effect on soot generation of the higher turbulent temperature fluctuations in the stagnation point region and in the hot sites below it in case 4 (see Fig. 8(f)), should be taken into consideration.

Although clearly higher overall amounts of soot are generated in the PI-region in case 4, the higher air mass flow rate (hence enhanced mixing rates) in this case leads to a high enough fuel and soot oxidation rates, which render fuel and soot concentrations in the upper parts of the furnace noticeably lower than those corresponding to case 1. In contrast to case 1, almost no unburned fuel or soot escape the furnace exit.

It should be noted that higher local temperatures in the flame front locations in case 4 are partly due to lower radiation heat losses from these locations. This can be confirmed by considering Figs. 5 and 6, where the clearly lower soot loading in the hot sites along the symmetry plane (see Fig. 5) leads to a significant reduction in the radiation heat loss from these sites (cf. Fig. 6).

8. Effect of increasing air injection velocity under fixed excess air ratio conditions (EAR = 1.15) (case 5)

In this subsection case 5 (Figs. 2(e) and 9) will be discussed; see Table 1. Hereby the effect of increasing the total amount of air entering the furnace under fixed overall EAR conditions, on combustion and soot processes, is investigated.

As compared with case 1, increasing the injection velocity of the combustion air in case 5 leads to higher amounts of hot gases which circulate from the stagnation point region downward (compare Figs. 2(a) and 2(e)). At the same time however, although the air injection velocity in case 5 is clearly higher than that corresponding to case 4 (see Table 1), in the later case a larger mass of hot gases is circulated downward into the PI-region. This is attributed to a larger amount of fuel admitted to the furnace in case 5. This leads to higher mass which tries to escape to the upper parts of the furnace by pushing air jets upward, particularly in the stagnation point region. Thereby the ability of the hot gases in the stagnation point region to penetrate downward is weakened. In the upper part of the furnace in case 5 the velocity and turbulence levels, hence the reaction rates are higher than those corresponding to case 1.

The temperatures, fuel concentrations and soot number densities in the contact sites between the fuel and air jets and in the stagnation point region are comparable in both cases 1 and 5. Local temperatures and fuel concentrations in the PI-region, closely below the stagnation point, are however somewhat higher in case 5 (cf. Figs. 3(a) and (b) and 9(a) and (b)). Nevertheless, in case 1 peak soot volume fraction levels in the PI-region are clearly higher. This might be explained by considering the flow fields of both cases (Figs. 2(a) and 2(e)). In case 5 soot precursors transferred downward into the PI-region penetrate, as compared with case 1, at a faster rate towards the primary inlet. Hence, their residence time in the hot fuel-rich soot formation favoring locations below the stagnation point region, is shortened. This faster penetration is due to the stronger circulating motion in the PI-region in case 5. After approaching the second stagnation point region formed closely above the primary inlet (see Fig. 2 (e)), in their subsequent travel upward towards the air jets, soot particles cover, as compared with the particles in case 1, a longer distance, under comparatively cool conditions (cf. Figs. 2(e) and 9(a)). In case 5 a larger proportion of the upwardly moving particles is entrained into the air jets at sites further separated from the stagnation point region (compare Figs. 2(a) and 2(e)). This will lower the probability of these particles to be circulated once more towards the stagnation point region, and then downward, hence to contribute subsequently more effectively to the soot formation activity in the PI-region. In other words, the probability that these particles will be entrained into the gas stream flowing upward, increases. On the other hand, in case 1 soot nuclei expelled from the stagnation point region in the downward direction, circulate at a lower speed in smaller vortices close to the stagnation point region (cf. Figs. 2(a) and 2(e)). Hence, their residence time in hot fuel-rich soot generation favoring locations is longer than that available for soot particles in the PI-region in case 5.

It should be noted that arguments mentioned above concerning the decreased residence time in soot formation promoting regions due to the stronger circulating currents in case 5 are also applicable in case 4. In this later case, however, the high soot concentration levels seen in the PI-region are attributed mainly to the clearly high number of soot particles transferred from the stagnation point region towards the PI-region (cf. Fig. 8(d)).

In the upper part of the furnace along the y–z plane local temperatures in case 5 are noticeably higher than those corresponding to case 1. This is mainly due to the

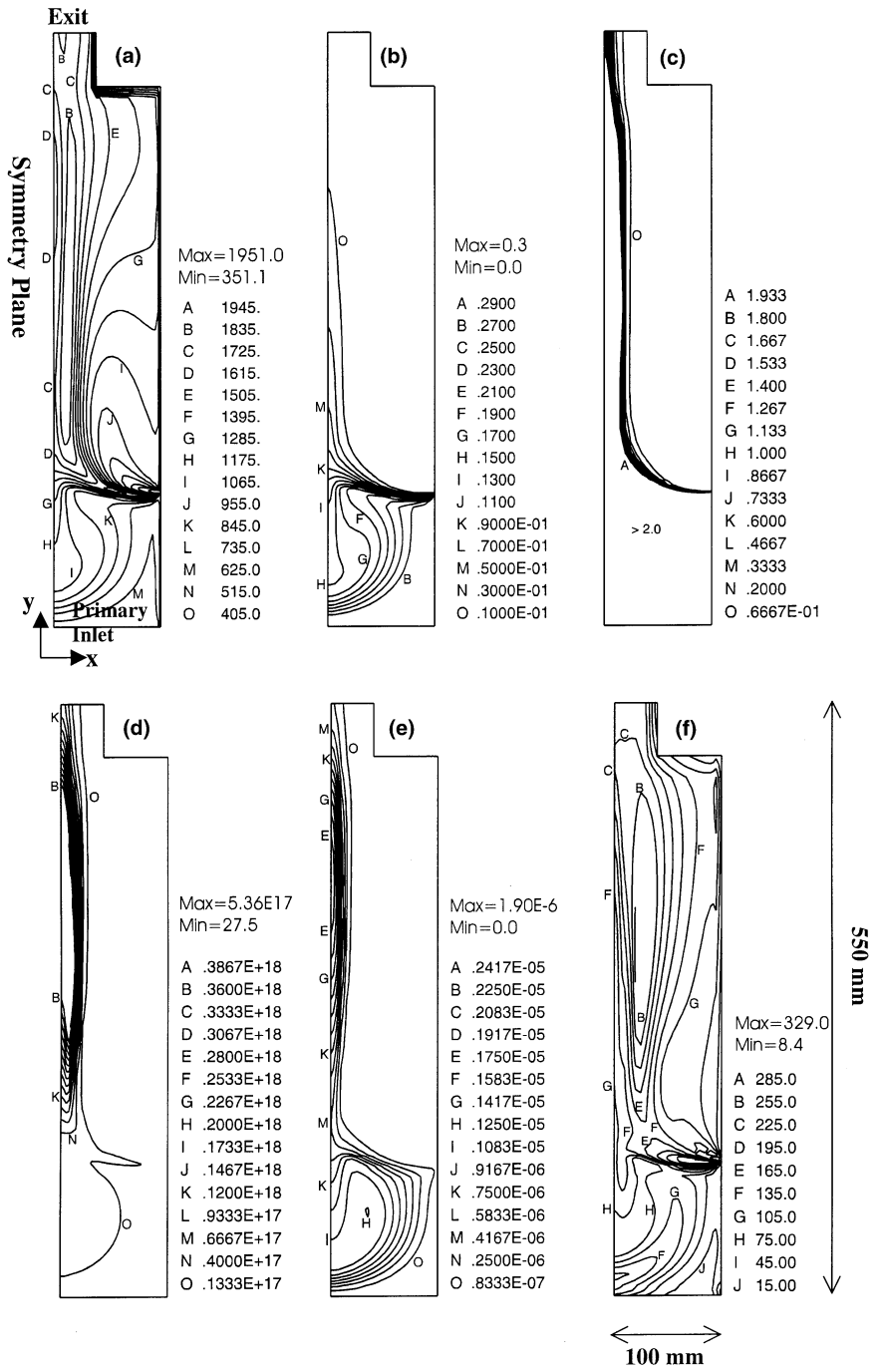

Fig. 9. Results for case 5: (a) temperature (K); (b) CH_4 mass fraction; (c) CH_4 equivalence ratio; (d) soot number density (part./m^3); (e) soot volume fraction; (f) $(\overline{T'^2})^{1/2}$.

higher level of turbulence mixing, hence more intensive combustion activity, caused by the higher overall mass flow rates in case 5. Although lower soot loading along the y–z plane in case 5 (cf. Fig. 5) is expected to adversely affect the heat radiated to walls, the clearly higher local temperatures in these sites counter this adverse effect and lead, as compared with case 1, to higher incident radiation flux at the walls (see Fig. 6). Moreover, although in case 5 the higher temperatures in the fuel-rich locations along the y–z plane enhance soot inception (compare

Figs. 3(d) and 9(d)), the higher flow velocities shorten the residence time available for newly generated soot particles to grow up in size to the extent which might enable them to show a significant contribution to soot loading in the sites of their existence. This represents a main factor leading to lower peak levels of soot volume fraction in case 5 (compare Figs. 3(e) and 9(e)).

As can be seen from Figs. 3(c) and (e) and Figs. 9(c) and (e), slightly higher amounts of methane and soot are emitted from the furnace in case 5. It should be remembered however that even when soot and fuel concentrations at the furnace exit are the same in both cases, total mass of pollutants exiting the furnace in case 5 is two times higher; total mass flow rate in the furnace in case 5 is two times greater than that corresponding to case 1.

9. Summary and conclusions

Combustion and soot processes in a small vertical methane-fueled furnace supplied with fuel through its primary inlet located at its bottom, and with air via two air jets issuing from two opposing rectangular slots extending horizontally in the direction of the depth of the furnace (z-direction in Fig. 1) are investigated numerically. The effect of the following operation parameters on soot processes is studied: (1) increasing the inlet temperature of both combustion air and fuel, (2) increasing the overall EAR, and (3) increasing the total mass flow rate of both air and fuel supplied to the furnace, under constant EAR conditions (i.e., increasing the output thermal power under fixed EAR conditions).

Based on the simulation results under the boundary conditions considered in this study, the following conclusions concerning the above-mentioned parameters, can be drawn:

(1) Increasing the inlet temperature of combustion air enhances soot inception in the stagnation point region formed midway between the two air jets. This leads also to larger and hotter circulating motions in the region located between the air jets and the primary inlet; referred to here as the PI-region. As a result of these two points soot production in this PI-region is enhanced significantly. In the upper parts of the furnace, however, soot concentrations are reduced due to the enhanced soot oxidation. Nevertheless, radiation heat transfer to the walls, which depends greatly on soot loading, is still clearly higher than that corresponding to the lower inlet air temperature cases. This is attributed to the higher local gas temperatures attained in the hot soot loaded sites when the inlet air temperature is increased.

(2) Decreasing the temperature of the fuel-bearing gas entering the furnace from its primary inlet leads to a clear reduction in the size of the hot circulating motions in the PI-region, as well as to decreasing soot inception both in the contact sites between the air jets and the fuel, and in the stagnation point region. Consequently, the total amounts of soot generated in the PI-region are reduced clearly. The resulting reduction is soot loading along all of the furnace height leads to a clear reduction in the total thermal energy radiated to the furnace walls.

(3) Increasing the overall EAR leads to higher temperatures in the stagnation point region, hence higher soot number densities, and to larger hot circulating motions in the PI-region. Consequently soot formation in the PI-region is enhanced significantly. However, due to the increase in EAR, soot loading in the upper part of the furnace is reduced by oxidation significantly. This has clear adverse consequences on the heat radiated to furnace walls.

(4) Increasing the total amount of air entering the furnace under fixed overall EAR conditions enhances combustion rates, hence leads to an increase in local temperatures. Total amounts of soot generated in the PI-region are increased due to arguments similar to those mentioned in the previous conclusion. However, in this case the peak levels of soot volume fraction in the hot fuel-rich sites are lower than those corresponding to the case when lower total amounts of gas are flowing in the furnace under the same overall EAR conditions. This is mainly due to the shorter residence time of soot particles in a hot soot generation favoring environment, dictated by the higher flow velocities in the former case. Irrespective of the lower peak levels of soot concentrations, heat radiated to the walls is enhanced when the amount of air admitted to the furnace is increased under fixed EAR conditions. This is attributed to the higher local temperatures attained due to the enhanced combustion rates in this case.

(5) Under the flow and combustion conditions considered in this study large enough amounts of soot are generated in the furnace which might indicate that ignoring a complete coupling between the gas phase and soot is not warranted if a sufficiently accurate prediction of the species concentrations and/or of the heat transfer by radiation is required.

References

[1] S.B. Al-Omari, K. Kawajiri, On the combustion and soot processes in a fluidized bed – like furnace, Combustion Science and Technology 154 (2000) 179–206.

[2] K.J. Syed, C.D. Stewart, J.B. Moss, Modelling soot formation and thermal radiation in buoyant turbulent diffusion flames, in: 23rd Symposium (International) on Combustion, The Combustion Institute, Pittsburgh, PA, 1990, pp. 1533–1541.

[3] J. Nagle, R.F. Strickland-Constable, Oxidation of carbon between 1000–2000 C°, in: Proceedings of the Fifth Conference on Carbon, Pergamon, New York, 1962, pp. 154–164.

[4] B.S. Haynes, Soot and hydrocarbons in combustion, in: W. Bartok, A.F. Sarofim (Eds.), Fossil Fuel Combustion, Wiley, New York, 1991, pp. 5.261–5.326.
[5] B.S. Haynes, H.G.G. Wagner, Soot formation, Prog. Energy Combust. Sci. 7 (1981) 229–273.
[6] C. Kapalan, C.R. Shaddix, K.C. Smyth, Computations of enhanced soot productin in time-varying CH_4/air diffusion flames, Combustion Flame 106 (1996) 392–405.
[7] B.F. Magnussen, B.H. Hjertager, On mathematical modeling of turbulent combustion with special emphasis on soot formation and combustion, in: 16th Symposium (International) on Combustion, The Combustion Institute, Pittsburgh, PA, 1976, pp. 719–729.
[8] F.C. Lockwood, N.G. Shah, A new radiation solution method for incorporation in general combustion prediction procedures, in: 18th Symposium (International) on Combustion, The Combustion Institute, Pittsburgh, PA, 1981, pp. 1405–1414.
[9] S.J. Brookes, J.B. Moss, Measurements of soot production and thermal radiation from confined turbulent jet diffusion flames of methane, Combustion Flame 116 (1999) 49–61.
[10] J.H. Kent, D.R. Honnery, A Soot formation rate map for a laminar ethylene diffusion flame, Combustion Flame 79 (1990) 287–299.